A Theoretical Redesign of ImplanTec®'s Compression Cerclage and Stabilisation System to Improve Clinical Outcomes of Fracture Fixation

Benjamin Peterson, JoJo Peplinski, Hope Mickey, and Kian Hageman

BME:5101 Biomaterials and Implant Design – Fall 2025

Professor Kallemeyn

Background

Fracture fixation is a technique employed to facilitate the healing process of a fractured bone. For minor fractures, splinting and casts are often sufficient for mending a fractured bone; for displaced or severe fractures, surgical intervention may be necessary. For surgical fracture fixation, there are many implanted devices on the market that achieve the goals of restoring natural anatomical positioning and mechanical stability of fractured bone. Stabilizing the fractured bone in its proper anatomical positioning expedites the natural process of fracture healing and, ordinarily, successfully restores function to the bones. Elements of fixation including stiffness, alignment, flexibility, and promotion of callus formation must be carefully balanced for fruitful fracture fixation (Epari et al., 2013). Fracture fixation has a storied history of implementation that has undergone drastic changes from its early renditions.

Cerclage wiring is one of the earliest documented methods of internal fixation, with the first reported use of metal wire for stabilizing fractures appearing in 1775 when French surgeons used brass wire to suture bone fragments (Hernigou & Pariat, 2016). Throughout the late 18th and 19th centuries, cerclage rapidly became the predominant fixation technique, leading Laurent Berenger-Feraud to write the first text on internal fixation in 1870; this text identified cerclage as the most efficient early operative method for stabilizing bone fragments (Hernigou & Pariat, 2016). As antiseptic techniques improved, particularly through Lister's discoveries in the 1860s, cerclage wiring transitioned from a high-risk intervention reserved for only open fractures and nonunion fractures to a practical, reproducible surgical technique (Hernigou & Pariat, 2016). By the late 19th century, it was routinely used to achieve direct immobilization, reduce micromotion at fracture sites, and support early functional recovery. Building from these early developments, modern orthopedic fixation expanded into four primary wire-based techniques: tension band wiring, full cerclage, hemi-cerclage, and interfragmentary wiring. Each method applies the principle of mechanically stabilizing bone fragments with controlled compression or constraint. Each method can also be used in combination with plates, intramedullary nails, or other fixation components. These wire

systems continue to play essential roles in durable long-term stabilization strategies in certain fracture patterns.

Fracture fixation with cerclage and related wire techniques remains a valuable methodology in modern orthopedic surgery, particularly for fracture patterns and intra-operative conditions where conventional screw fixation is not possible or where proper fragment positioning is difficult to obtain (Agarwala et al., 2017). Stand-alone cerclage loops have limited strength and are therefore most often used with axial or splinting devices like Steinman pins, plates, or nails (Agarwala et al., 2017). These help to increase rotational and bending stability. Clinically, cerclage wire fixation carries risks: malalignment, local infection, wire migration, delayed union, wire breakage, and occasionally neurovascular injury (Lenz et al., 2012). These risks mean that special attention must be given to technique and implant choice. Specific indications where cerclage provides the most benefit include unstable intertrochanteric and certain acetabular fracture patterns, fixation of periprosthetic femoral fractures, the stabilization of osteotomized or trochanteric fragments during THA revision, and instances where screw fixation is precluded or where cortical bone is thin (Lenz et al., 2012). In shoulder and elbow periprosthetic or metaphyseal fractures, cerclage wires offer a useful supplemental option where plate or screw placement is compromised (Grechenig et al., 2017). Modern advances have produced percutaneous and minimally invasive (MIPO) cerclage routes which reduce exposure, infection risk, and vascular damage (Förch et al., 2021). Together, this historical evolution and broad range of contemporary clinical applications illustrate how cerclage fixation has remained a versatile and lasting component to fracture management across diverse anatomical and surgical contexts. Figure 1 shows the ImplanTec® Compression Cerclage and Stabilisation System in a radiograph of its usage for an isolated fracture of the femur.

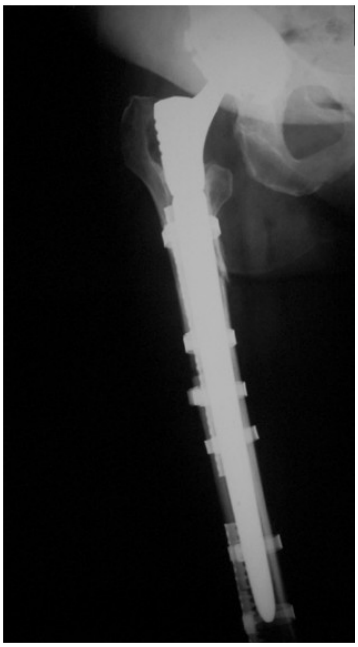

Figure 1: ImplanTec® Compression Cerclage and Stabilisation System in radiograph (ImplanTec, n.d.).

Rationale/Motivation

Cerclage wiring is a well-established fixation technique with extensive historical use. Cerclage wires may be placed at fracture sites where the bone has lost significant density or at periprosthetic fracture sites; in both cases, using other typical securements such as bone screws would not be feasible (Angelini & Battiato, 2015). One of the more common applications is for fixation of periprosthetic fracture in the femur after total hip arthroplasty. The prevalence of periprosthetic fracture after total hip arthroplasty may be as high as 18% (Capone et al., 2017). Cerclage wiring is also recommended for intraoperative fractures

of the proximal femur, which occur in 3.5% of cementless arthroplasties and 17.6% of revision procedures (Angelini & Battiato, 2015). With the significant need for effective fracture fixation and an increasing rate of periprosthetic fractures there is apparent reason to develop an effective fracture fixation device (Lenz et al., 2013). Improvements to existing cerclage fixation devices or methods will improve patient outcomes by reducing the rate of device failure and preventing further surgical procedures.

Problem Definition

The current gold standard for periprosthetic or osteoporotic fracture fixation is cerclage wiring. There is a variety of configurations for cerclage wiring; the wire itself might be solid or multi-stranded cable and can be single-looped, double-looped, or braided, then closed by a crimp, twist, knot, half-knot with twists, or hairpin knot (Angelini & Battiato, 2015). A diagram of these configurations is shown below, in Figure 2. Of these procedures, a twist closure is the most clinically applied, although the hairpin knot yields much higher compressive force and tensile strength in comparison (Angelini & Battiato, 2015). A major characteristic of the success of fixation is the stability of the wire. This stability is characterized into three groups: absolute stability, with no displacement and solid unity of the fracture, relative stability, with reversible displacement occurring when a fracture is loaded, and “loose-lock stability,” with free displacement when the wire is not under tension and resisted displacement under tension (Angelini & Battiato, 2015).

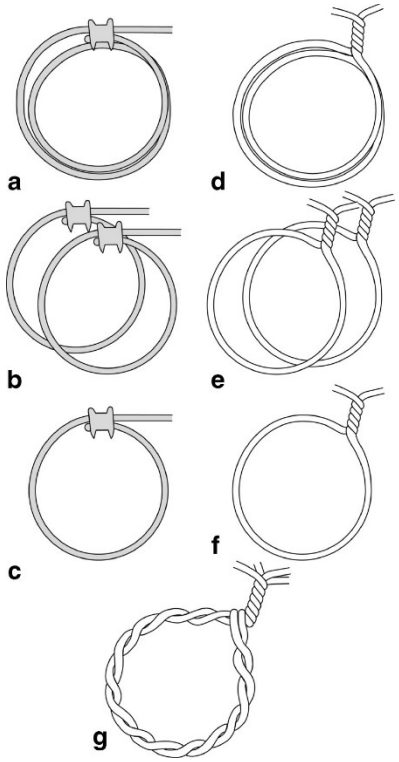

Figure 2: Cerclage wire configurations (Lenz et al., 2013). Diagrams a-c show crimp closures while diagrams d-g show twist closures. Diagrams a and d show double-looped cable cerclages. Diagram g shows two braided wire cerclage cables.

While the clinical use of cerclage wiring is extensive, cerclage cables themselves are associated with a high failure rate (Ménard et al., 2013). Lack of tension and gradual loosening can result in cerclage wire slacking or slipping (Angelini & Battiato, 2015). Unfortunately, loosening is very common, even across multiple cerclage wire designs (Ménard et al., 2013). The slipping and subsequent micromotion of the wire(s) can cause the fracture to become misaligned, which introduces increased risk of additional fracture or other detrimental effects such as bone resorption and damage to the periosteal blood supply (Angelini & Battiato, 2015). Additional surgeries to rectify the effects of loosening also put the patient at an increased risk of health complications.

An additional solution is the Compression Cerclage and Stabilisation System (CCG), which utilizes a flatter band-like design rather than a wire (ImpanTec, n.d.). This design increases the contact area at the interface between the band and the bone, and the band fastener allows for easy control of compression. This addresses the primary issue of cerclage wiring, which is prone to loosening even at insertion. The CCG also may incorporate a stabilizer, which increases frictional resistance of the overall system and encourages osseointegration with its rough texture and titanium composition (ImplanTec, n.d.). The full system is shown below in Figure 3. The CCG bands themselves utilize a rough blasted titanium surface and fixation spikes for stability.

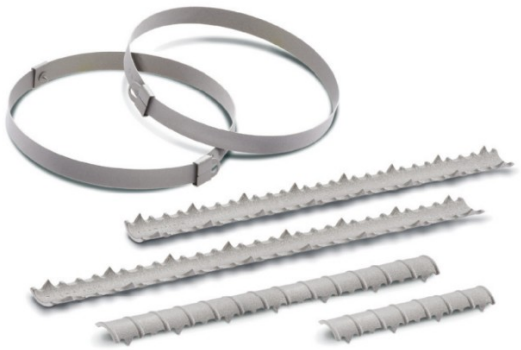

Figure 3: ImplanTec® Compression Cerclage and Stabilisation System (ImplanTec, n.d.).

With an increase in the prevalence of periprosthetic fracture, it is vital that there is a successful fixation technique available. Existing solutions do not sufficiently address the risk of micromotion, loosening and slippage, and pose increased risk of infection, failure, and other complications. Overall, there is a need for a device which securely fixes fracture sites without damage to the periosteum.

Design Requirements

The redesigned cerclage system must meet several functional requirements and constraints to ensure mechanical reliability, biological safety, and clinical usability. Mechanically, the device should demonstrate reduced displacement under typical loading relative to current devices, withstand at least 280 N of tensile load (Visser et al., 2025), and maintain stability under cyclical loading with minimal micromotion. It must also provide increased friction at the bone-implant interface while preserving periosteal blood flow by maintaining stable point or line contact without generating excessive circumferential pressure. Biocompatibility and corrosion resistance are essential, particularly when used alongside titanium components. The design should minimize infection risk and minimize soft-tissue irritation by avoiding sharp edges and excessive prominence. Clinically, the system must be radiographically identifiable, compatible with existing cerclage instrumentation or require only minimal surgical workflow modifications, and allow safe intraoperative tensioning without risk of breakage, deformation, or cortical injury. Finally, the device should accommodate anatomical variability in bone curvature and diameter and remain fully removable during revision surgery without damaging surrounding bone or soft tissue.

Design Concept

The design incorporates channels to allow for periosteum blood flow. The design has smooth edges with convex raised sections to reduce stress concentration and sharp edges that may damage bone. Within each raised section, Sharklet®-inspired patterns are applied in multiple orientations to increase friction and reduce micromotion in all directions. The Sharklet® microtexture is ordinarily utilized to help improve microbial resistance (Mann et al., 2014). In using this pattern on a greater scale, we expect our designed pattern to improve infection resistance and to increase static friction between the cerclage system and the bone reducing the probability of micromotion. Micromotion increases the chance of bone damage and fracture fixation failure, primarily by loosening (Pankaj & Xie, 2019; Wazen et al., 2013). The increased surface texture and overall roughness should increase friction and reduce slippage, loosening, and

micromotion. Integrating these design considerations should improve patient outcomes and reduce revision rates and need for additional surgical procedures.

Figures 4-7 show the key features of our redesign with a laser-melted surface pattern that helps increase friction while potentially retaining the Sharklet® pattern's inherent microbial resistance. Throughout this report, the texture we designed is referred to as a microtexture. However, it is important to note that this is a relative term, and Abebi and his team refer to a texture on a similar scale as a macrotexture in their report because their research included an even smaller scale (Abadi et al., 2025).

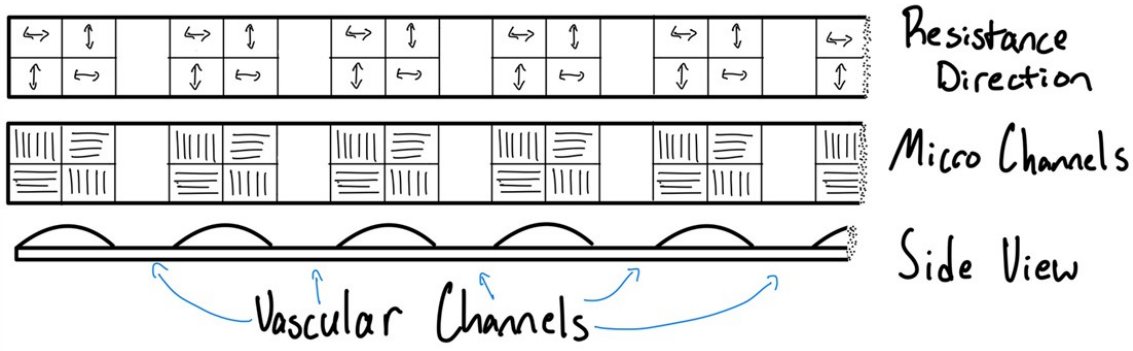

Figure 4: Preliminary sketches of microtexture pattern and cerclage band design.

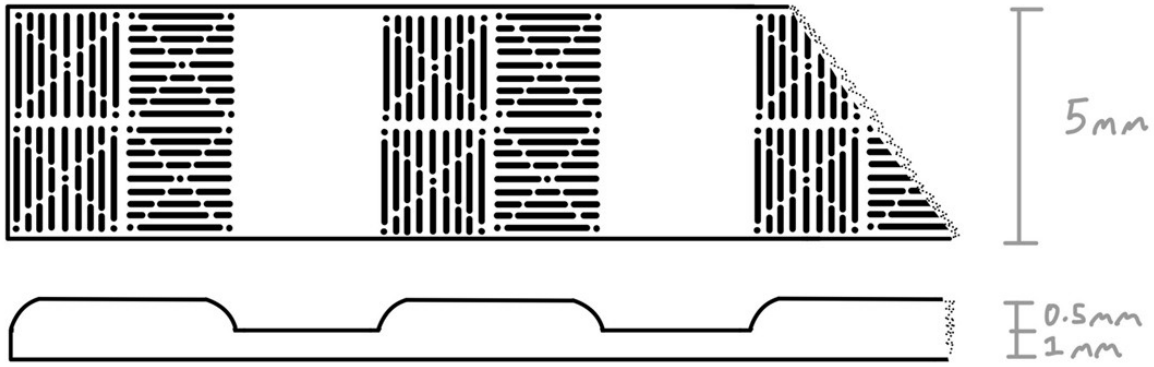

Figure 5: Detailed sketch of proposed cerclage band design and micropattern.

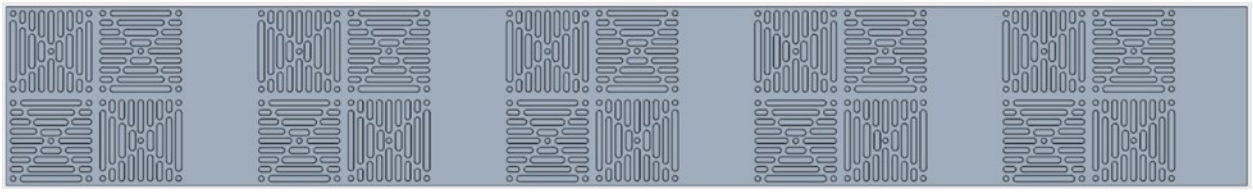

Figure 6: CREO Parametric model of the interfacing side of the device. The four-quadrant pattern alternates between two resisting orientations and has space to accommodate vascular channels.

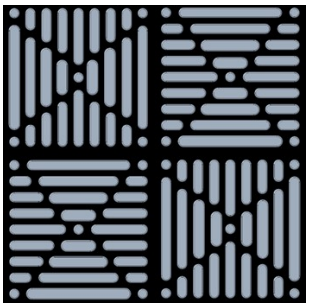

Figure 7: Expanded view of the surface microtexture. The pattern for each quadrant is the same but is rotated 90° in the top left and bottom right quadrants. The black background allows for a better visualization of the pattern.

For the redesign of ImplanTec®'s titanium (Ti-6Al-4V) Compression Cerclage and Stabilisation system, titanium remains an appropriate material choice because of its excellent biocompatibility, corrosion resistance, and compatibility with the titanium plates and components commonly used in modern fracture and periprosthetic fixation. Although historical analyses show that stainless steel wires have the best mechanical strength and that vitallium exhibits the highest tensile strength, these materials introduce concerns for galvanic corrosion when interacting with titanium implants (Angelini & Battiato, 2015). Devices made from cobalt-chromium or titanium alloys have been shown to provide adequate stability when used as adjuncts rather than primary load-bearing elements (Angelini & Battiato, 2015). Biocompatibility of the material is also a major concern here. One requirement of cerclage systems is the preservation of periosteal blood flow. Studies of the cerclage-bone interface demonstrate that traditional cerclage systems achieve fixation through narrow line or point contacts while leaving adjacent "spanned zones" unloaded, which protects periosteal circulation and prevents circumferential cortical strangulation (Lenz et al., 2012). Our design builds on this biological principle by incorporating regularly spaced channels on the inner surface of the band intended to maintain essential perfusion pathways while increasing friction and reducing micromotion compared to a smooth circumferential band. Between these channels, the microtextured surface serves as the point contacts.

When selecting a surface texture for our design, we considered a range of engineering and bio-inspired patterns reported in fracture fixation literature. Prior studies have examined how different micro- and macro-scale textures influence tribological behavior, particularly the coefficient of friction (COF). For example, Xu et al. investigated how sliding direction affects COF on laser-textured titanium featuring a stacked-ring pattern. Their work showed that the COF increased in all orientations except when sliding occurred along the stacked ring direction (Costa et al., 2021). This pattern is shown in Figure 8. Second, Rung et al. compared frictional behavior of two laser-generated surface textures on steel: low-frequency Laser-Induced Periodic Surface Structures (LIPSS) and micro-channels (Figure 9). Their findings indicated that low-frequency LIPSS consistently produced a higher COF regardless of sliding direction. However, the micro-channels produced a similar COF when under a higher force (Costa et al., 2021). Abedi et al. examined a range of textured patterns on Ti-6Al-4V (Figure 10) sliding against bone and found that all textures increased COF relative to an untextured surface, with a lined pattern producing the highest friction (2025). Wang et al. used femtosecond laser processing to fabricate micro-grooves on steel and studied the effect of groove spacing on friction. Compared to an untreated surface, COF increased for periodicities between 15-25μm, then decreased with further spacing increases. Moreover, several research groups have also drawn inspiration from nature. Sánchez et al. analyzed snakeskin and found that friction against balsa wood varied with sliding direction (Figure 11), with motion from tail to head generating a higher COF (Costa et al., 2021; Sánchez et al., 2021). Another bio-inspired approach is the Sharklet® micropattern (Figure 12) which, as its name implies, is modeled after sharkskin. Although its primary benefit lies in reducing bacterial contamination, its structured micro-geometry informed several of our design considerations (Mann et al., 2014).

Based on these patterns, our team developed several preliminary concepts. These included a honeycomb-inspired texture incorporating the Sharklet® surface within each hexagon, a repeated "peanut-shaped" geometry, and a design consisting of intersecting V-shaped grooves oriented toward a central point while preserving channels for vascularization. Ultimately, we combined these ideas by retaining the vascular channels and incorporating a rotatable texture pattern designed to resist slipping in all directions. We were particularly motivated by the demonstrated reduction in bacterial contamination of the Sharklet® pattern and the consistently high COF achieved by simpler lined or grooved textures. Our final concept integrates both: a rotated primary geometry with friction-enhancing grooves, with its shape inspired by Sharklet®. The final pattern (Figure 7) is intended to be manufactured using selective laser melting.

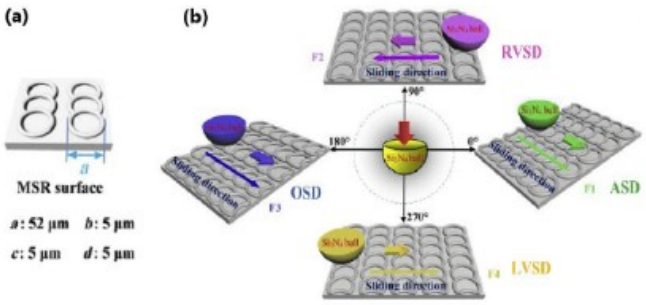

Figure 8: (left) Stacked-ring texture created by laser surface texturing. (right) Four sliding directions evaluated in Xu et al.'s study (Costa et al., 2021).

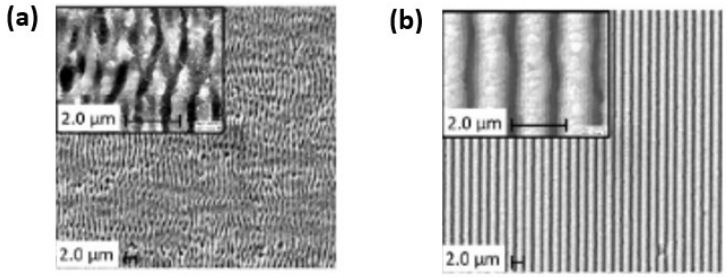

Figure 9: (left) Low-frequency Laser-Induced Periodic Surface Structures (LIPSS). (right) Micro-channel texture used for comparison (Costa et al., 2021) .

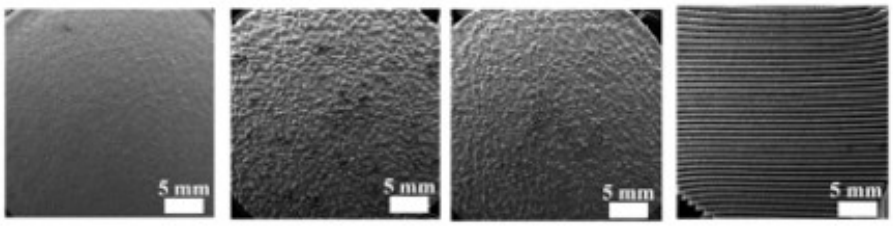

Figure 10: Textured Ti-6Al-4V samples ranging from untextured (left) to increasing roughness (middle) and micro-grooves (right) in Abedi et al. (2025).

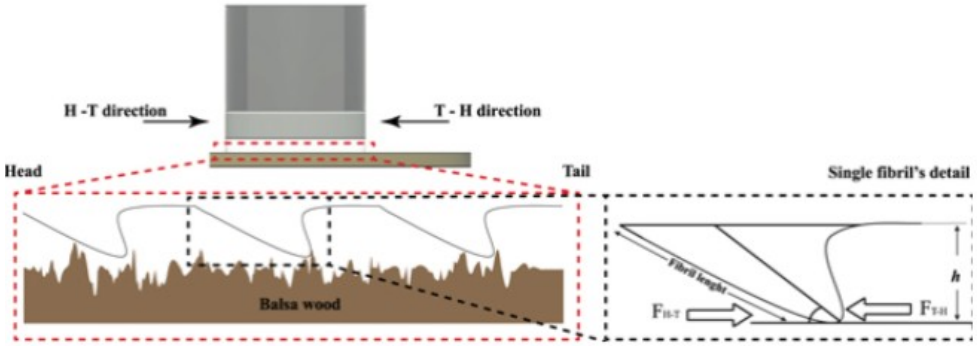

Figure 11: Diagram of the test apparatus used to evaluate frictional behavior of snakeskin, showing the direction-dependent sliding paths (Sánchez et al., 2021).

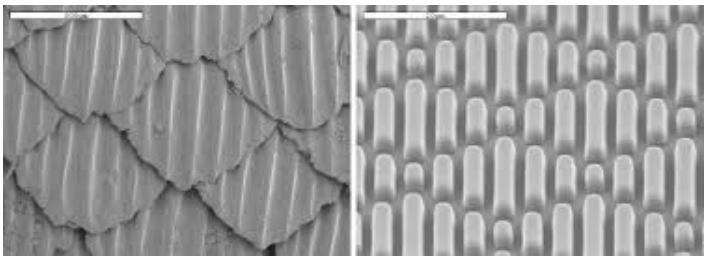

Figure 12: Natural sharkskin microstructure (left) (scale bar 500 µm). Engineered Sharklet® micropattern derived from sharkskin (right) (scale bar 20 µm) ("Technology Overview," n.d.).

Analysis

The increased frictional resistance from the micropattern created on the device combined with the force distribution properties of the wider band will help reduce slippage and micromotion. Micromotion of the cerclage system is undesirable because it increases the likelihood for cortical and soft tissue damage, which can lead to fibrous encapsulation and implant loosening (Wazen et al., 2013). Continuous micromotion causes progressive loosening and can lead to mechanical failure of the fracture fixation (Pankaj & Xie, 2019). For this reason, a device design which increases bone-implant frictional resistance to micromotion is vital.

Our design involves an increase in the COF with adding microtexture on a titanium band compared to a smooth titanium band. A study addressing the frictional behavior of bone and various metals with varying surface textures provides the basis for our analysis (Abedi et al., 2025). Table 1 below shows an extraction of their findings, including the COF between bone and both polished titanium and "Macro-Featured" saw tooth; in their study, when they applied a 0.5 MPa load they found bone on polished titanium to have a COF of 0.19 and bone on titanium with a sawtooth texture to have a COF of 0.87. With this information, we developed a Creo Simulate model to show the change in displacement and stress distribution due to differing COFs between the bone and fixation methods.

Table 1: An extraction from Abedi et al, 2025 table one.

Ti-6Al-4V	Ra (µm)	Bone Type (g/cm^3)	Stress (MPa)	Mean COF
Polished	0.11	Femur	0.1-0.12	0.16
	N/A		0.15-1	0.19
	0.1±0.0		0.1-2.5	0.42
Macro-Featured	Lattice	Femur	0.15-1	0.9
	Sawtooth	Humerus (D = 0.1-0.4)	0.5/1.0/1.5	0.93/0.77/0.67
		Humerus (D = 0.4-0.7)		0.87/0.73/0.63
		Humerus (D = 0.7-0.1)		0.83/0.57/0.37

The pressure caused by cerclage wire forces is typically measured *in vitro* by sawing a bone sample in half, placing pressure sensors or bars on the inside, then securing the wires and measuring the forces. The range of forces measured in the literature is wide, from 40 N to 280 N (Koo et al., 2015; Visser et al., 2025). For our model, the maximum force of 280 N is used. In terms of geometric properties, we used the average male superior transverse diameter of the femur is 33 mm, which corresponds to a circumference of 103mm (Polguj et al., 2013). The typical cerclage wire is 1 mm wide, and our band is 5 mm wide, which results in a 103 mm^2 wire surface area and a 515 mm^2 band surface area. This causes a wire pressure of 2.42 MPa and band pressure of 0.54 MPa, which is a 4/5 reduction in pressure. The pressure of 0.54 MPa used in the model permits us to use the previously discussed COF for a stress of 0.5 MPa. Other model properties such as material properties, constraints, and forces are noted in Table 2.

Table 2: Material properties used in the simulation.

Part	Bone	Source	Polished Ti	Source	Textured Ti	Source
Material	Bone		Ti-6Al-4V		Ti-6Al-4V	
Density	1.3 g/cm^2	(International Commission on Radiological Protection et al., 2001)	4.43 g/cm^2	(*ASM Material Data Sheet*, n.d.)	4.43 g/cm^2	(*ASM Material Data Sheet*, n.d.)
Poisson's Ratio	0.3	(Lai et al., 2015)	0.33	(*ASM Material Data Sheet*, n.d.)	0.33	(*ASM Material Data Sheet*, n.d.)
Young's Modulus	17 GPa	(Lai et al., 2015)	113.8 GPa	(*ASM Material Data Sheet*, n.d.)	113.8 GPa	(*ASM Material Data Sheet*, n.d.)
Tensile Yield Stress	100 MPa	(Baleani et al., 2024)	880 MPa	(*ASM Material Data Sheet*, n.d.)	880 MPa	(*ASM Material Data Sheet*, n.d.)
Tensile Ultimate Stress	160 MPa	(Riggs et al., 1993)	950 MPa	(*ASM Material Data Sheet*, n.d.)	950 MPa	(*ASM Material Data Sheet*, n.d.)
COF with bone at 0.5N	X	X	0.42	(Abedi et al., 2025)	0.87	(Abedi et al., 2025)
Pressure Applied	X	X	0.5 MPa	Calculated	0.5 MPa	Calculated

The goal of the simulation is to better understand the stresses put on the bone that are caused by the different COFs. The setup for the simulation is shown in Figure 13, with a fixed block of bone and two titanium bands placed on its surface. Material properties based on literature values were assigned to the bone and titanium bands as shown in Figure 14. Friction between the materials was assigned with an interface definition between the bottom surface of the titanium and top surface of the bone as seen in Figure 15. The two titanium plates are constrained to only move across the bone in the Z direction.

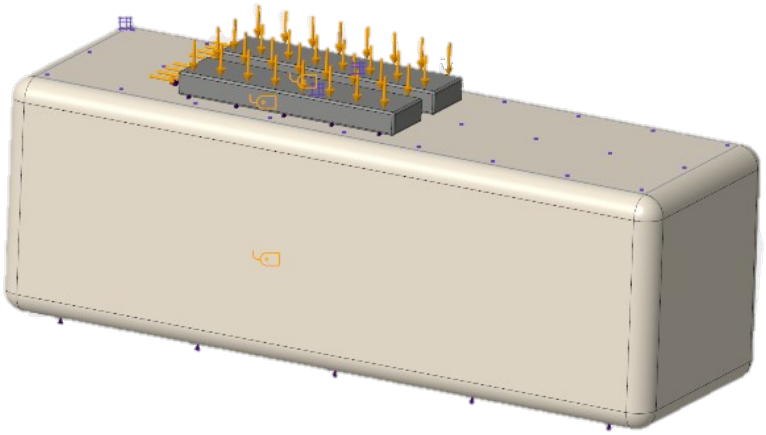

Figure 13: Creo model with polished and sawtooth titanium places, bone block, material tags, and forces.

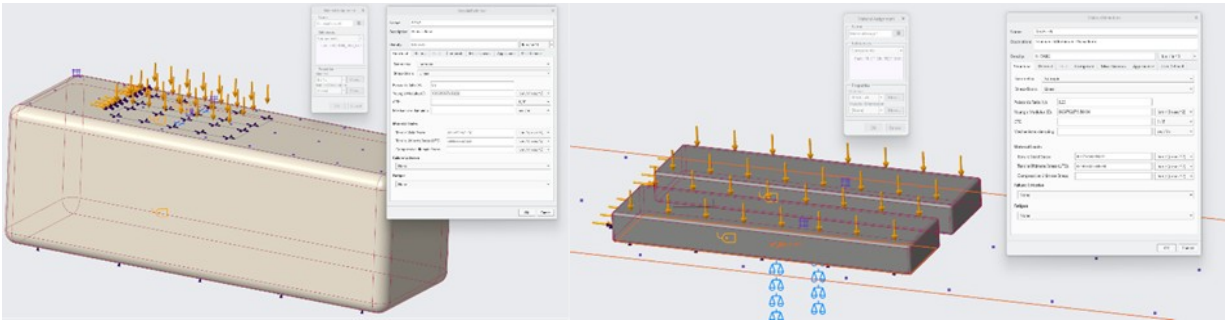

Figure 14: Creo Model showing material properties and assignments for titanium bands and bone block.

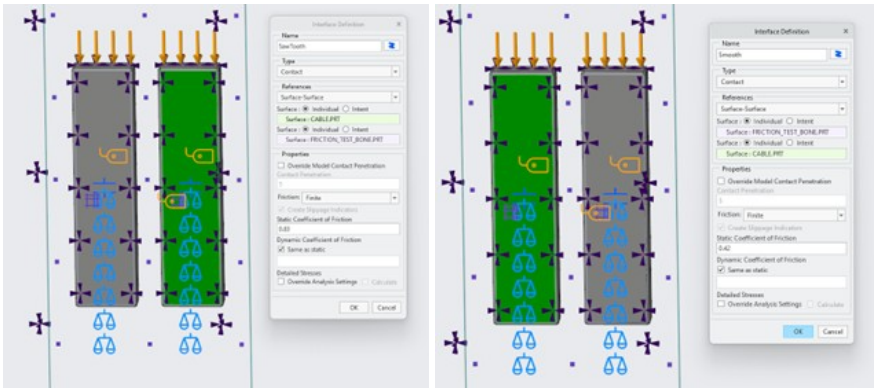

Figure 15: Interface definitions of the sawtooth (left) and smooth (right) titanium plates.

Figure 16 shows the forces applied to the model to determine corresponding slippage and contact forces. A force of 100 N was applied on the edge to simulate movement. A mesh was then formed for the objects; the top of the bone and the titanium plates were refined with a 0.1 mm max constraint. This mesh is composed of 1,354 cells with an orthogonal quality of 0.548. Figure 17 shows a mesh visualization.

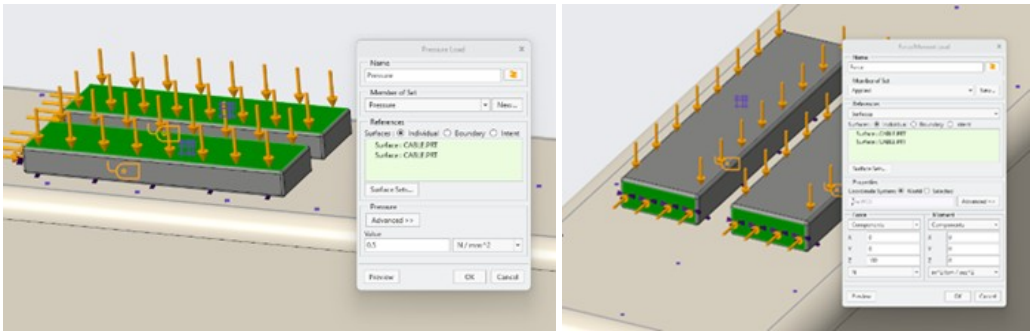

Figure 16: Creo model showing pressures applied to the Ti-6Al-4V titanium. Downward pressure (left) is applied to resemble the tight clamping force around the bone and lateral force (right) is applied to determine slippage.

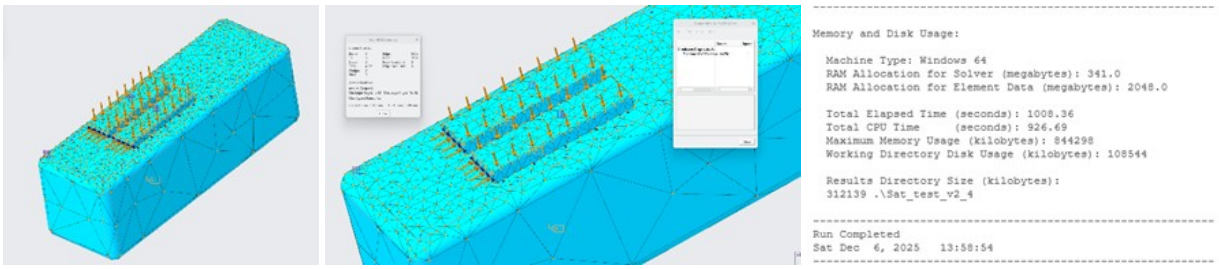

Figure 16: Images of Creo Simulate model showing the mesh created for the study (left and center) and the solved mesh computer usage (right).

The Von Mises stress distribution over the surface of the bone is shown in Figure 18. The model has been made primarily transparent to improve visibility of stress under the Ti-6Al-4V samples.

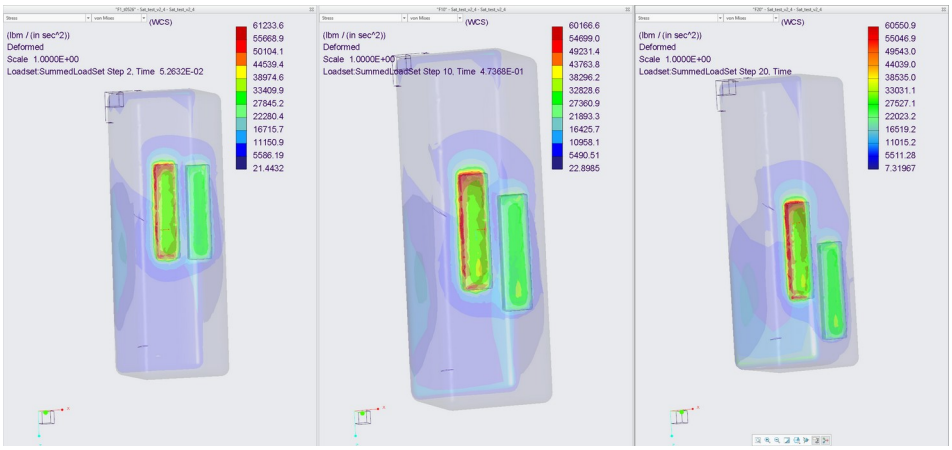

Figure 17: Frames 2,10, and 20 of the simulation with bone and Ti-6Al-4V plates transparent. This shows the Von Mises stresses generated as a result of surface interactions. For all images, the left plate represents our microtextured device and the right plate represents device with a polished surface.

Our device is a modification of pre-existing devices whose general reliability, safety, and effectiveness have been established in the medical industry. Our device is designed to be a one-time use comprised of biocompatible Ti-6Al-4V titanium alloy that is industry standard. As a bone fixation cerclage device, our device falls under Food and Drug Administration (FDA) regulation number 888.3010 and the device is classified as Class II and device code 4530 (21 CFR 888.3010 -- Bone Fixation Cerclage., n.d.; Fixation Cerclage FDA Classification, Life Cycle Events [4530], n.d.). Devices like ours fall under the 510K pathway for market approval with the FDA, which means there are clear standards for testing and approvals. To that end, Advancing Standards Transforming Markets (ASTM) has developed standard F2180, last updated in 2024, that sets the standard specification for metallic implantable strands and cables (ASTM International, 2024). This references the test methods and material specifications. ASTM F136-13 sets the standard for the wrought Ti-6AL-4V alloy for surgical implant applications (ASTM International, 2021). The standards for surface preparation and marking of metallic surgical implants are outlined in ASTM F86 (ASTM International, 2021).

To evaluate our device, ASTM standard F2180 and F136-13 reference ASTM E8/E8M for tension testing (ASTM International, 2021, 2024). ASTM F136-13 also references ASTM E290 for bend testing for material ductility and various standards for alloy purity testing (ASTM International, 2025). Our device should meet these standards and undergo these testing procedures. Standard ASTM E8 outlines tension testing, including parameters such as standard dimensions of test pieces, allowable precision tolerances, and methods of data collection and analysis. Additionally, our design requires comprehensive frictional testing. This testing should consist of a fractured bone affixed with our device then pulled, pushed, and twisted on both ends (in separate studies) to create stress on the band; next, measurements of the deformation of the band, device slippage, and more should be recorded. This process should be repeated for multiple trials with multiple bone fracture types. Testing should also be executed with industry standard cables, wires, and bands. A comparison of slippage prevention or reduction between industry standard devices and our device would prove if our design successfully improved fixation.

Unfortunately, the additional manufacturing step of laser surface texturing makes our device more costly compared to the current market standard cables, wires, and bands. For reference, a standard 1 mm cerclage wire costs $66.34 and a cerclage band system costs $142 (gSource, 2025; WestCMR, 2025). We expect our device to cost slightly more than the average cerclage band set.

Fortunately, the clinical implementation of a microtextured cerclage band would require minimal adjustments to standard surgical technique. Dedicated instrumentation, such as a compatible passer and tensioning device, may be necessary to ensure proper orientation of the device relative to the bone; the longitudinal channels which allow blood flow over the periosteum and textured surface must be

interfacing with the bone to provide a stable friction-enhancing fixation without the excessive circumferential compression known to impair cortical vascularity. In using similar technology to the ImplanTec® CCG we ensure the device remains fully removable with standard tools and does not require complicating revision procedures while preserving reliability comparable to existing cerclage systems.

References

21 CFR 888.3010 -- Bone fixation cerclage. (n.d.). https://www.ecfr.gov/current/title-21/chapter-I/subchapter-H/part-888/subpart-D/section-888.3010

Abedi, A., Farahmand, F., Salmanimehrjardi, M., & Nasiri Khonsari, H. (2025). Frictional behavior between bone and additively manufactured Ti6Al4V implants is affected by bone density and surface texture under varying loads. Scientific Reports, 15(1), 41620. https://doi.org/10.1038/s41598-025-25586-0

Agarwala, S., Menon, A., & Chaudhari, S. (2017). Cerclage wiring as an adjunct for the treatment of femur fractures: Series of 11 cases. *pmc.ncbi.nlm.nih.gov*. https://doi.org/10.13107/jocr.2250-0685.842

Angelini, A., & Battiato, C. (2015). Past and present of the use of cerclage wires in orthopedics. European Journal of Orthopaedic Surgery & Traumatology, 25(4), 623–635. https://doi.org/10.1007/s00590-014-1520-2

ASM Material Data Sheet. (n.d.). Retrieved December 7, 2025, from https://asm.matweb.com/search/specificmaterial.asp?bassnum=mtp641

ASTM International. (2021). Standard Practice for Surface Preparation and Marking of Metallic Surgical Implants F86. United States: World Trade Organization Technical Barriers to Trade Committee.

ASTM International. (2024). Standard Specification for Metallic Implantable Strands and Cables F2180. United States: United States: World Trade Organization Technical Barriers to Trade Committee.

ASTM International. (2025). Standard Test Methods for Tension Testing of Metallic Materials E8/E8M. United States: World Trade Organization Technical Barriers to Trade Committee.

ASTM International. (2021). Standard Specification for Wrought Titanium-6Aluminum-4Vanadium ELI (Extra Low Interstitial) Alloy for Surgical Implant Applications (UNSR56401). World Trade Organization Technical Barriers to Trade Committee.

Baleani, M., Erani, P., Acciaioli, A., & Schileo, E. (2024). Tensile Yield Strain of Human Cortical Bone from the Femoral Diaphysis Is Constant among Healthy Adults and across the Anatomical Quadrants. Bioengineering, 11(4), 395. https://doi.org/10.3390/bioengineering11040395

Capone, A., Congia, S., Civinini, R., & Marongiu, G. (2017). Periprosthetic fractures: Epidemiology and current treatment. Clinical Cases in Mineral and Bone Metabolism: The Official Journal of the Italian Society of Osteoporosis, Mineral Metabolism, and Skeletal Diseases, 14(2), 189–196. https://doi.org/10.11138/ccmbm/2017.14.1.189

Costa, H. L., Schille, J., & Rosenkranz, A. (2021). (PDF) Tailored surface textures to increase friction—A review. ResearchGate. https://doi.org/10.1007/s40544-021-0589-y

Fixation cerclage FDA Classification, Life cycle events [4530]. (n.d.). Https://fda.report/Product-Code/deviceId/4530

Förch, S., Reuter, J., Von Der Helm, F., Lisitano, L., Hartwig, C., Sandriesser, S., Nuber, S., & Mayr, E. (2021). A minimally invasive cerclage of the tibia in a modified Goetze technique: operative technique and first clinical results. *European Journal of Trauma and Emergency Surgery*, *48*(4), 3115–3122. https://doi.org/10.1007/s00068-021-01857-z

Grechenig, S., Hohenberger, G., Bakota, B., Staresinic, M., Grechenig, P., & Ernstberger, A. (2017). Humeral shaft cerclage wiring: a safe technique to prevent radial nerve injury. *Injury*, *48*, S12–S14. https://doi.org/10.1016/s0020-1383(17)30732-5

gSource. (2025). Cerclage Wire 1.0mm x 10 meters 19 gauge. https://www.gsource.com/instruments/orthopedic/orthopedic-cerclage-wire/cerclage-wire-orthopedic-cerclage-wire/cerclage-wire-1-0mm-x-10-meters-19-gauge/

Hernigou, P., & Pariat, J. (2016). History of internal fixation (part 1): early developments with wires and plates before World War II. *International Orthopaedics*, *41*(6), 1273–1283. https://doi.org/10.1007/s00264-016-3347-4

ImplanTec. (n.d.). CCG – The compression cerclage and stabilisation system [Brochure]. https://www.hb-medical.nl/wp-content/uploads/HB_CCGSystem-brochure-Surgical-Technique.pdf

International Commission on Radiological Protection, Clarke, R. H., NutionL! Rutliological Prorection Board, Dr. L.-E. Holm, Dr. J. Valentin, R. Alexaklrin, J. D. Boice Jr., R. Cox, G. J. Dicus, C. Streffer, A. Sugier, Z. Pan, B. C. Winkler, B. Lindell, C. B. Meinhold, W. K. Sinclair, L. S. Taylor, A. J. Gonzlalez, D. Beninson, . . . H. J. Dunster. (2001). Annals of the ICRP. ICRP, 22. https://psec.uchicago.edu/Simulation/icrpp89.pdf?

Koo, K., Zhou, Z., Yew, A. K., Koh, J. S., & Howe, T. S. (2015). A Biomechanical Study Comparing Cerclage Wiring Performed with a Power Tool versus the Manual Method. Annals of the Academy of Medicine, Singapore, 44(12), 554–557. https://doi.org/10.47102/annals-acadmedsg.V44N12p554

Lai, Y.-S., Chen, W.-C., Huang, C.-H., Cheng, C.-K., Chan, K.-K., & Chang, T.-K. (2015). The Effect of Graft Strength on Knee Laxity and Graft In-Situ Forces after Posterior Cruciate Ligament Reconstruction. PLOS ONE, 10(5), e0127293. https://doi.org/10.1371/journal.pone.0127293

Lenz, M., Perren, S. M., Gueorguiev, B., Richards, R. G., Krause, F., Dell'Oca, A. F., Höntzsch, D., & Windolf, M. (2012). Underneath the cerclage: an ex vivo study on the cerclage-bone interface mechanics. *Archives of Orthopaedic and Trauma Surgery*, *132*(10), 1467–1472. https://doi.org/10.1007/s00402-012-1572-x

Lenz, M., Perren, S. M., Richards, R. G., Mückley, T., Hofmann, G. O., Gueorguiev, B., & Windolf, M. (2013). Biomechanical performance of different cable and wire cerclage configurations. *International orthopaedics*, *37*(1), 125–130. https://doi.org/10.1007/s00264-012-1702-7

Mann, E. E., Manna, D., Mettetal, M. R., May, R. M., Dannemiller, E. M., Chung, K. K., Brennan, A. B., & Reddy, S. T. (2014). Surface micropattern limits bacterial contamination. Antimicrobial Resistance and Infection Control, 3, 28. https://doi.org/10.1186/2047-2994-3-28

Ménard, J., Émard, M., Canet, F., Brailovski, V., Petit, Y., & Laflamme, G. Y. (2013). Initial Tension Loss in Cerclage Cables. The Journal of Arthroplasty, 28(9), 1509–1512. https://doi.org/10.1016/j.arth.2013.03.014

Pankaj, P., & Xie, S. (2019). The risk of loosening of extramedullary fracture fixation devices. *Injury*, *50*, S66–S72. https://doi.org/10.1016/j.injury.2019.03.051

Polguj, M., Bliźniewska, K., Jędrzejewski, K., Majos, A., & Topol, M. (2013). Morphological study of linea aspera variations – proposal of classification and sexual dimorphism. Folia Morphologica, 72(1), 72–77. https://doi.org/10.5603/FM.2013.0012

Riggs, C. M., Vaughan, L. C., Evans, G. P., Lanyon, L. E., & Boyde, A. (1993). Mechanical implications of collagen fibre orientation in cortical bone of the equine radius. Anatomy and Embryology, 187(3), 239–248. https://doi.org/10.1007/BF00195761

Sánchez, J. C., Estupiñán, H., & Toro, A. (2021). Friction response of bioinspired AISI 52100 steel surfaces texturized by photochemical machining. Surface Topography: Metrology and Properties, 9(1), 014001. https://doi.org/10.1088/2051-672X/abe090

Technology Overview. (n.d.). Sharklet Technologies, Inc. Retrieved December 6, 2025, from https://www.sharklet.com/technology-overview/

Visser, D., Bliemel, C., Schürholz, T., Aigner, R., Ruchholtz, S., & Bäumlein, M. (2025). Wire cerclages as part of osteosynthesis- examination for optimal placement. Archives of Orthopaedic and Trauma Surgery, 145(1), 228. https://doi.org/10.1007/s00402-025-05795-y

Wazen, R. M., Currey, J. A., Guo, H., Brunski, J. B., Helms, J. A., & Nanci, A. (2013). Micromotion-induced strain fields influence early stages of repair at bone–implant interfaces. *Acta Biomaterialia*, *9*(5), 6663–6674. https://doi.org/10.1016/j.actbio.2013.01.014

WestCMR. (2025). ARTHREX: AR-7820TB. https://www.westcmr.com/ar-7820tb-we1-ar-7820tb?srsltid=AfmBOooBED5-cIS-YoCHGVC9rQ235pHKe_M9qEhBOltbjfkombSUsrX3&